POLITECNICO
MILANO 1863

SCUOLA DI INGEGNERIA INDUSTRIALE
E DELL'INFORMAZIONE

Executive Summary of the Thesis

Finding regions of bounded motion in binary asteroid environments using Lagrangian Descriptors

Laurea Magistrale in Space Engineering - Ingegneria Spaziale

Author: Sebastiano Raffa

Advisor: Prof. Francesco Topputo

Co-advisor: Gianmario Merisio

Academic year: 2021-2022

1. Introduction

A binary asteroid environment is characterized by a low-gravity field where small dynamical perturbations affect significantly the dynamics [3]. Consequently, trajectory design for space exploration missions targeting small solar system bodies is challenging, especially for spacecraft with a limited control authority. In the near future, two missions part of the Asteroid Impact and Deflection Assessment (AIDA) international collaboration are scheduled to visit the (65803) Didymos binary system: NASA's DART, and ESA's Hera. The former is expected to conduct a kinetic impact experiment on the smaller body Dimorphos, while the latter is expected to study the effects of the impact. They both plan on deploying CubeSats in the proximity of the Didymos system, therefore raising the need for methods to find quasi-periodic, bounded orbits in the proximity of the double asteroid.

The circular restricted three-body problem (CR3BP) is far from being representative of the dynamical environment close to the Didymos–Dimorphos system. A perturbed bi-elliptic restricted four-body problem (BER4BP) including solar radiation pressure (SRP) is better suited for a more accurate representation of the real dynamics. However, periodic orbits around Didymos vanish in the perturbed BER4BP since the problem is non-autonomous and only quasi-periodic solutions exist.

The goal of the paper is to show how Lagrangian descriptors (LDs) [5] can conveniently reveal regions of bounded motion in double asteroid environment. For this purpose, resonant periodic orbits about the secondary are computed in the CR3BP starting from a family of distant retrograde orbits (DROs) through differential correction and inspected against the LD scalar field for regions classification. The LD scalar field of the perturbed BER4BP is visually examined to identify solutions that persist about Dimorphos. Results indicate that regions of bounded motion still exist, regardless of the perturbations. Overall, LDs provide insightful dynamical information and are more efficient than other chaos indicators typically used in astrodynamics, which usually require the computation of the state transition matrix.

2. Equations of motion

The perturbed bi-elliptic restricted four-body problem (PBER4BP) asks for the motion of

a particle in a gravitational field generated by three massive bodies moving in elliptical orbits and exposed to the SRP perturbation.
Let the primaries be Didymos (D1) and Dimorphos (D2). The model is expressed in the synodic reference frame centered at the primaries barycenter, which rotates and pulsates to keep their distance equal to one [4]. Let $\mu = m_{D2}/(m_{D1} + m_{D2})$, where m_{D1} and m_{D2} are the masses of D1 and D2, respectively. The positions of D1 and D2 are (-μ, 0, 0) and (1-μ, 0, 0), respectively. The equations of motion (EoM) are scaled such that the sum of D1 and D2 masses is set to one as well as their distance, and their period is scaled to 2π [4].
By designating the primaries true anomaly f as the independent variable of the system, the EoM are [3, 4]

$$\ddot{\mathbf{r}} + \begin{bmatrix} 0 & -2 & 0 \\ 2 & 0 & 0 \\ 0 & 0 & 0 \end{bmatrix} \dot{\mathbf{r}} = \nabla\Omega + \alpha \left(\frac{\mathbf{r}_S}{\|\mathbf{r}_S\|^3} - \frac{\mathbf{r}+\mathbf{r}_S}{\|\mathbf{r}+\mathbf{r}_S\|^3} \right) + \beta \frac{\mathbf{r}+\mathbf{r}_S}{\|\mathbf{r}+\mathbf{r}_S\|^3} \quad (1)$$

$$\dot{\theta} = \gamma \frac{(1+e_S\cos\theta)^2}{(1-e_S^2)^{3/2}} \frac{(1-e_D^2)^{3/2}}{(1+e_D\cos f)^2} \quad (2)$$

where $\dot{(\cdot)}$ and $\ddot{(\cdot)}$ denote the first and second derivatives with respect to the true anomaly f; θ is the true anomaly of the double asteroid barycenter (D) with respect to the Sun (S) and its derivative is obtained through the chain rule [4]; $\mathbf{r} = (x, y, z)$ and $\mathbf{r}_S = (x_S, y_S, z_S)$ are the non-dimensional position vectors of the spacecraft and the Sun, respectively, expressed in the synodic reference frame; $\mu_{(\cdot)}$, $a_{(\cdot)}$, and $e_{(\cdot)}$ refer to the gravitational parameter, the semi-major axis, and the eccentricity of the body $(\cdot)$, respectively (see Table 1). Then, Ω is the potential function that reads:

$$\Omega = \frac{1}{1+e_D\cos f}\left[\frac{1}{2}(x^2+y^2-z^2 e_D\cos f) + \frac{1-\mu}{r_{D1}} + \frac{\mu}{r_{D2}}\right] \quad (3)$$

where r_{D1} and r_{D2} are the distances from Didymos and Dimorphos, respectively. The nondimensional coefficients α, β, and γ are computed as

$$\alpha = \frac{\mathrm{TU}^2}{\mathrm{LU}^3}\mu_S, \quad \beta = \frac{\mathrm{TU}^2}{\mathrm{LU}^3}\frac{P_0 d_{\mathrm{AU}}^2 C_r A}{m},$$
$$\gamma = \sqrt{\frac{\mu_S+\mu_D}{\mu_D}\left(\frac{a_D}{a_S}\right)^3},$$

where $P_0 = 4.56\,\mathrm{N\,km^{-2}}$ is the solar radiation pressure at 1 AU; $d_{\mathrm{AU}} = 149\,597\,870.700\,\mathrm{km}$ is the Astronomical Unit; $C_r = 1.2$ is the assumed reflectivity coefficient; $A = 1.8\,\mathrm{m}^2$ is the assumed Sun-projected area on the spacecraft for SRP evaluation; $m = 10\,\mathrm{kg}$ is the assumed spacecraft mass. TU and LU are the normalization factors given by

$$\mathrm{TU} = \sqrt{\frac{a_D^3}{\mu_D}}\frac{(1-e_D^2)^{\frac{3}{2}}}{(1+e_D\cos f)^2},$$
$$\mathrm{LU} = \frac{a_D(1-e_D^2)}{1+e_D\cos f}.$$

The Sun position vector is retrieved according to

$$\mathbf{r}_S = \mathbf{A}_1\,\mathbf{A}_2\,\frac{1}{\mathrm{LU}}\frac{a_S(1-e_S^2)}{(1+e_S\cos\theta)}\begin{bmatrix}\cos\theta \\ \sin\theta \\ 0\end{bmatrix}. \quad (4)$$

where $\mathbf{A}_2$ is the rotation matrix from the heliocentric perifocal to the ecliptic frame and $\mathbf{A}_1$

Table 1: Parameters related to Didymos–Dimorphos binary system.

Physical Parameters			Heliocentric Orbit			Binary Orbit		
	Unit	Value		Unit	Value		Unit	Value
μ	-	$9.214\,228 \times 10^{-3}$	e_S	0.38384		e_D	0.03	
μ_D	$\mathrm{km^3\,s^{-2}}$	$3.522\,601 \times 10^{-8}$	a_S	1.64420	AU	a_D	1.19 ± 0.03	km
μ_S	$\mathrm{km^3\,s^{-2}}$	$1.327\,124 \times 10^{11}$	i_S	3.40795	deg	i_D	174	deg
-	-	-	Ω_S	73.19580	deg	Ω_D	40	deg
-	-	-	ω_S	319.32295	deg	ω_D	0 (assumed)	deg
-	-	-	T_S	770.07519	Days	T_D	11.920+0.004/-0.006	Hours

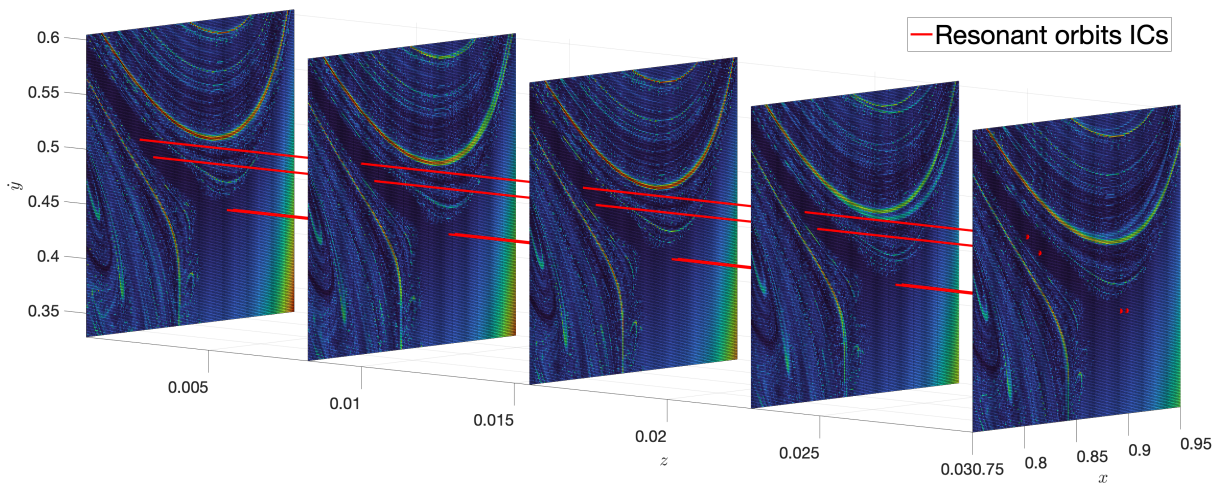

Figure 1: LD scalar field in the CR3BP at different z slices.

maps the rotation from the ecliptic to the rotating pulsating reference system. These transformations are computed as in [1], with the parameters in Table 1.

3. Methodology

3.1. Lagrangian descriptors

LDs allow investigating the geometric pattern of structures that govern transport in phase space. Their definition and heuristic arguments explaining why they are effective are presented in [5]. In this study, we used the following LD definition

$$M(\mathbf{x}_0, f_f) = \int_0^{f_f} |\mathcal{F}(\mathbf{x}(f))| \, \mathrm{d}f, \tag{5}$$

where $|\mathcal{F}(\mathbf{x}(f))| = \|\dot{\mathbf{x}}\|$ is a positive bounded scalar, $\mathbf{x} = [x, y, z, \dot{x}, \dot{y}, \dot{z}]^\top$ is the phase space state and $\dot{\mathbf{x}} = [\dot{x}, \dot{y}, \dot{z}, \ddot{x}, \ddot{y}, \ddot{z}]^\top$ is its derivative. In [5], an extensive class of different LDs was defined based on the integrand, the selected norm, and the integration interval. In this work, we use one LD that is computed with forward integration, since we are interested in the future evolution of initial conditions (ICs). The LD is computed appending its integrand to the space state equations with a zero initial value and propagating the extended dynamics.

3.2. Spatial resonant periodic orbits

In the circular problem, bifurcations from a planar family of distant retrograde orbits (DROs) generate spatial resonant periodic orbits [2]. To build them, the eigenvalues and eigenvectors of the monodromy matrix of planar periodic solutions are required. If λ_i and λ_i are complex conjugate eigenvalues, they can be written as $\lambda_i = \cos(\theta) + i\sin(\theta)$ and $\lambda_j = \cos(\theta) - i\sin(\theta)$, since $\lambda_i \cdot \lambda_j = 1$. This means that a small displacement in the direction described by the corresponding eigenvectors $\{\mathbf{e}_i, \mathbf{e}_j\}$, will rotate θ per period. These eigenvectors must have a component in the z and $\dot{z}$ directions in order to generate a close spatial resonant orbit. Moreover, after n revolutions on the reference orbit the small displacement must rotate such that $n\theta = 2\,k\pi$, where n and k are positive integers. In other terms

$$n = \frac{2\,k\,\pi}{\arccos\left[\frac{1}{2}(\lambda_i + \frac{1}{\lambda_i})\right]}. \tag{6}$$

As different planar periodic solutions (DROs) are considered, different integers of n and k can be obtained. Each orbit in the family will have a different couple (n, k), thus different resonances.

3.3. Finding regions of bounded motion

The process of searching for bounded orbits in the Didymos–Dimorphos system is made of two stages:

1. classification of the regions of the LD field through spatial resonant periodic solutions in the simplified, autonomous CR3BP starting from a planar family of DROs;

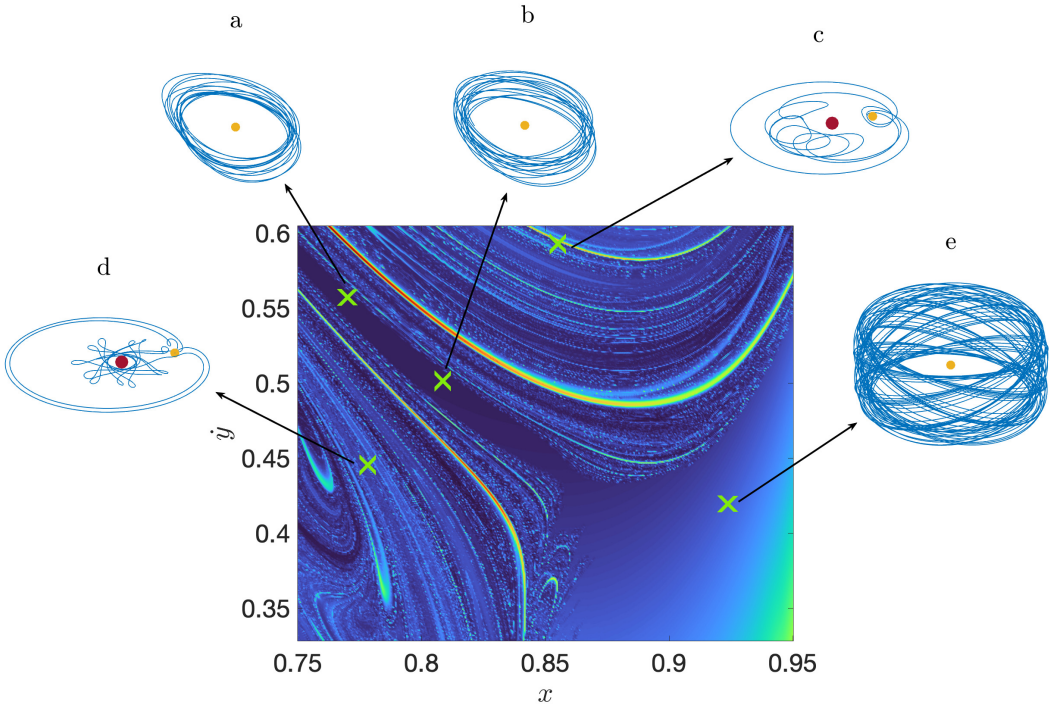

Figure 2: Sampling LD scalar field in the CR3BP. The red and yellow dots are Didymos and Dimorphos not to scale, respectively.

2. computation of the LD field within more representative, non-autonomous dynamical models, and phase space sampling to find bounded orbits.

Stage 1 seeks to discover spatial resonant periodic orbits in the CR3BP, whose ICs are inspected against the LD field, to ensure that they all fall within a smooth region of the scalar field. This serves to understand the behavior of the discovered regions which is unknown a priori. Four families of spatial periodic xz plane–symmetric orbits at different resonances are obtained by starting from a family of planar DROs and applying the techniques of *Differential Correction* and *Numerical Continuation* [2]. The latter algorithm is implemented by using the initial state's z_0 value as a continuation parameter, resulting in orbits with increasing z values. In stage 2, on the other hand, the LD field of the PBER4BP is sampled relying on the previously acquired information. Three major cases are investigated: first, the CR3BP described by Eq. 1, with $\alpha = 0$, $\beta = 0$, $e_D = 0$, and by replacing $f \to t$. Then, the BER4BP perturbed by the SRP, both when the Didymos–Dimorphos system is at the pericenter and apocenter of the heliocentric orbit. If regions of bounded motion still exist, they are expected to be similar to the ones found in stage 1. On the contrary, when they are lost, the LD scalar field is supposed to have a completely different look. ICs are propagated for ten primaries revolutions, hence from $f_0 = 0$ to $f_f = 20\pi$.

4. Results

The implemented grid consists of $400 \times 400 \times 5$ ICs along x,y, and z, respectively. In stage 1, as the grid is three-dimensional, the evolution of the LD field is observed at different non–dimensional z slices. The second stage plans to sample the phase space of the SRP perturbed BER4BP, in particular the highest–z slice ($z = 0.03$) of the LD field, to search for solutions that could potentially map the whole surface of Dimorphos. In this discussion, Didymos and Dimorphos are considered to be point masses, and physical collisions with them are not checked.

4.1. Classification of regions in the three-dimensional circular case

Results of stage 1 are shown in Fig. 1. The four red curves representing the resonant periodic orbits intersect the smooth region that extends from the bottom-right to the top-left corner of the $z =$ cost slice of the plot. The region nar-

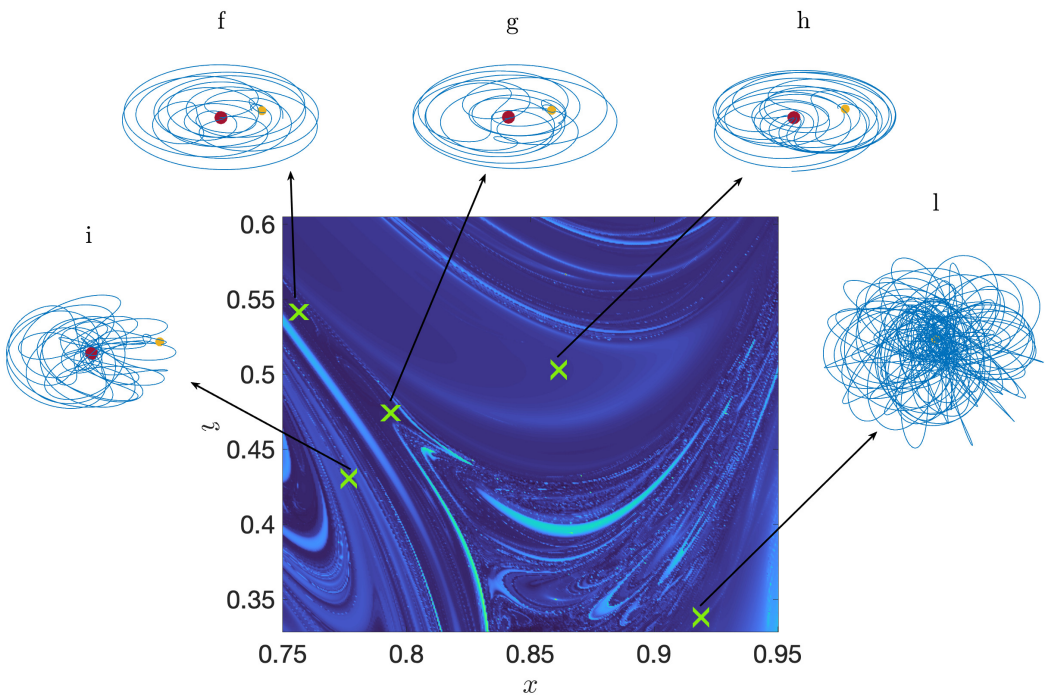

Figure 3: Samples evolution in the SRP perturbed BER4BP, for $\theta_0 = 0$. The red and yellow dots are Didymos and Dimorphos not to scale, respectively.

rows towards higher velocities and further distances from the secondary body. The smooth region is then thought to contain ICs that persistently revolve about Dimorphos. On its sides, on the other hand, chaotic regions appear: they are well-separated from the smooth region and are expected to contain only unbounded orbits. Five trajectories are sampled, three from the smooth region, and two from the rippled areas (see Fig. 2). The first three points (a, b, and e) exhibit bounded motion by behaving similarly to the family of resonant orbits previously found, while the other two (c and d) immediately escape the system.

4.2. Sampling in the perturbed bi-elliptic restricted four-body problem

The effect of the Sun is addressed in a more realistic model: the SRP perturbed bi-elliptic restricted four-body problem. Two cases are investigated, depending on the angular position θ_0 on the heliocentric orbit:

- Didymos–Dimorphos at the **pericenter** of the heliocentric orbit $\theta_0 = 0$, at 1.013 AU: this is the closest point to the Sun, where its perturbations are the greatest. The smooth region collecting ICs of bounded orbits is expected to be severely affected: the access to the vast selection of bounded orbits is likely to be no longer permitted;
- Didymos–Dimorphos at the **apocenter** of the heliocentric orbit $\theta_0 = \pi$, at 2.27 AU: at the farthest point from the Sun, it represents the best-case scenario as the magnitude of the perturbations is the lowest.

Figure 3 shows what the regions look like when the system is at the pericenter of the heliocentric orbit. The resulting LD field is heavily altered: unlike the CR3BP case, the separatrices are less pronounced; the two chaotic zones merge as they expand, taking up the entire phase space and incorporating the central channel that collected bounded orbits. Searching for bounded orbits through sampling becomes more challenging. The first points (f, g) are sampled near the central channel's previous location to verify if a fraction of the smooth region is still accessible. Points h and i sample the two extended chaotic areas, and the final point l is chosen to be pretty close to the secondary Dimorphos to exploit its gravitational attraction as much as possible. Almost all of the samples diverge: the effect of the SRP at the closest point to the Sun is so strong to sweep away any possible bounded motion, at least for the selected grid width. Sample l being

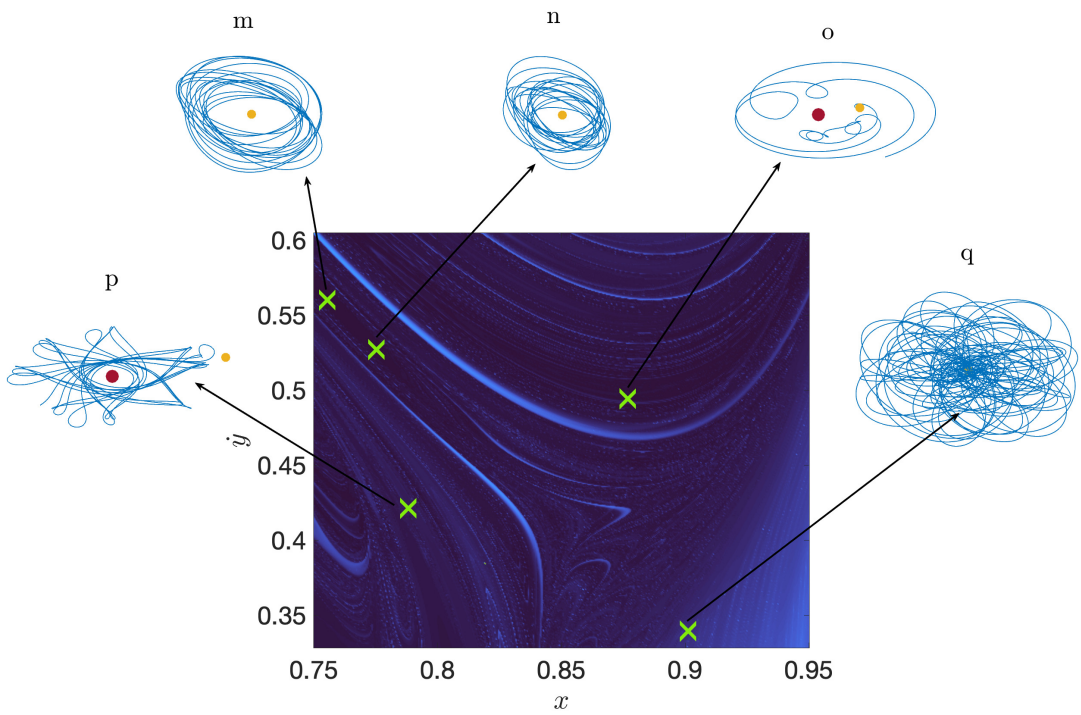

Figure 4: Samples evolution in the SRP perturbed BER4BP, for $\theta_0 = \pi$. The red and yellow dots are Didymos and Dimorphos not to scale, respectively.

so close to Dimorphos still revolves around it, but as already stated, physical impacts with the surface are not checked.

The best-case scenario, when the system is at the apocenter of its heliocentric orbit, is reported in Fig. 4. The structure of the LD resembles, yet differently scaled, the CR3BP case, with some differences to be noted. The entire smooth zone is broken down into two smaller regions, with chaotic behavior separating them. The first is a small portion of the channel that collects ICs of bounded orbits, in the top-left corner of the field: points m and n confirm the presence of bounded orbits in this region once more, regardless of the perturbations. The second is the wide smooth area located on the bottom-right in which trajectory q, which flies very close to Dimorphos, is likely to impact the surface multiple times. Samples o and p, belonging to the unstable areas, immediately escape the system.

When the system is at the pericenter of the heliocentric orbit, the stable regions vanish, only to reappear when the system travels away from the Sun.

5. Conclusion

This study looks into the effectiveness of LDs in revealing phase space organizing structures in binary asteroid environments. They demonstrate success in finding regions of bounded motion in non-autonomous dynamical models of the (65803) Didymos system. Features highlighted by the LD scalar field are classified through a preliminary inspection in the CR3BP. In the SRP perturbed BER4BP, while bounded motion areas can still be captured at the farthest point from the sun, they vanish at the pericenter of the heliocentric orbit: the SRP contribution is so strong to break down the majority of structures, leading to a vast region of chaotic motion. Ultimately, Lagrangian descriptors provide perceptive dynamical knowledge about the problem at hand more conveniently than other widespread chaos indicators used in astrodynamics for preliminary trajectory design.

References

[1] Nima Assadian and Seid H. Pourtakdoust. On the quasi-equilibria of the bielliptic four-body problem with non-coplanar motion of primaries. *Acta Astronautica*, 66(1):45–58,

2010.

[2] Hongru Chen, Elisabet Canalias, D. Hestroffer, and Xiyun Hou. Effective stability of quasi-satellite orbits in the spatial problem for phobos exploration. *Journal of Guidance, Control, and Dynamics*, 43:2309–2320, 08 2020.

[3] Fabio Ferrari, Vittorio Franzese, Mattia Pugliatti, Carmine Giordano, and Francesco Topputo. Trajectory Options for Hera's Milani CubeSat Around (65803) Didymos. *Journal of the Astronautical Sciences*, 68(4):973–994, December 2021.

[4] Nicola Hyeraci and Francesco Topputo. Method to design ballistic capture in the elliptic restricted three-body problem. *Journal of Guidance, Control, and Dynamics*, 33:1814–1823, 11 2010.

[5] Ana M. Mancho, Stephen Wiggins, Jezabel Curbelo, and Carolina Mendoza. Lagrangian descriptors: A method for revealing phase space structures of general time dependent dynamical systems. *Commun. Nonlinear. Sci. Numer. Simulat.*, 2013. `https://doi.org/10.1016/j.cnsns.2013.05.002`.